Orthogonal polynomials describing polarization aberration for rotationally symmetric optical systems

Xiangru Xu,[1,3] Wei Huang,[1,2,*] and Mingfei Xu[1,3]

[1]*Changchun Institute of Optics, Fine Mechanics and Physics, Chinese Academy of Sciences, Changchun, Jilin 130033, China*
[2]*State Key Laboratory of Applied Optics, Changchun, Jilin 130033, China*
[3]*University of Chinese Academy of Sciences, Beijing 100039, China*
[*]*huangw@ciomp.ac.cn*

Abstract: Optical lithography has approached a regime of high numerical aperture and wide field, where the impact of polarization aberration on imaging quality turns to be serious. Most of the existing studies focused on the distribution rule of polarization aberration on the pupil, and little attention had been paid to the field. In this paper, a new orthonormal set of polynomials is established to describe the polarization aberration of rotationally symmetric optical systems. The polynomials can simultaneously reveal the distribution rules of polarization aberration on the exit pupil and the field. Two examples are given to verify the polynomials.

©2015 Optical Society of America

OCIS codes: (220.3740) Lithography; (260.5430) Polarization; (080.1005) Aberration expansions.

References and links

1. J. Kye, G. R. McIntyre, Y. Norihiro, and H. J. Levinson, "Polarization aberration analysis in optical lithography systems," Proc. SPIE **6154**, 61540E (2006).
2. M. Shribak, S. Inoue, and R. Oldenbourg, "Polarization aberrations caused by differential transmission and phase shift in high-numerical-aperture lenses: theory, measurement, and rectification," Opt. Eng. **41**(5), 943–954 (2002).
3. R. A. Chipman, "Polarization aberrations," Ph.D. dissertation, Univ. of Arizona, (1987).
4. J. P. McGuire, Jr. and R. A. Chipman, "Polarization aberrations. 1. Rotationally symmetric optical systems," Appl. Opt. **33**(22), 5080–5100 (1994).
5. M. Totzeck, P. Graupner, T. Heil, A. Gohnermeier, O. Dittmann, D. Krahmer, V. Kamenov, J. Ruoff, and D. Flagello, "How to describe polarization influence on imaging," Proc. SPIE **5754**, 23–37 (2005).
6. G. R. McIntyre, J. Kye, H. Levinson, and A. R. Neureuther, "Polarization aberrations in hyper-numerical-aperture projection printing: a comparison of various representations," J. Micro. Nanolithogr. MEMS MOEMS **5**(3), 033001 (2006).
7. B. Geh, J. Ruoff, J. Zimmermann, P. Gräupner, M. Totzeck, M. Mengel, U. Hempelmann, and E. Schmitt-Weaver, "The impact of projection lens polarization properties on lithographic process at hyper-NA," Proc. SPIE **6520**, 65200F (2007).
8. J. Ruoff and M. Totzeck, "Orientation Zernike polynomials: a useful way to describe the polarization effects of optical imaging systems," J. Micro. Nanolithogr. MEMS MOEMS **8**(3), 031404 (2009).
9. J. Ruoff and M. Totzeck, "Using orientation Zernike polynomials to predict the imaging performance of optical systems with birefringent and partly polarizing components," Proc. SPIE **7652**, 76521T (2010).
10. Y. Shiode and T. Ebiahara, "Study of polarization aberration measurement using SPIN method," Proc. SPIE **6154**, 615431 (2006).
11. L. Dong, Y. Li, X. Dai, H. Liu, and K. Liu, "Measuring the polarization aberration of hyper-NA lens from the vector aerial image," Proc. SPIE **9283**, 928313 (2014).
12. Y. Tu, X. Wang, S. Li, and Y. Cao, "Analytical approach to the impact of polarization aberration on lithographic imaging," Opt. Lett. **37**(11), 2061–2063 (2012).
13. A. Serebriakov, F. Bociort, and J. Braat, "Correction of the phase retardation caused by intrinsic birefringence in deep UV lithography," Proc. SPIE **5754**, 1780–1791 (2005).
14. J. Sasián, "Polarization fields and wavefronts of two sheets for understanding polarization aberrations in optical imaging systems," Opt. Eng. **53**(3), 035102 (2014).
15. J. Dirk, "Projection exposure method, projection exposure system and projection objective," United States Patent US9036129 (2015).

#248659 Received 27 Aug 2015; revised 25 Sep 2015; accepted 30 Sep 2015; published 14 Oct 2015
© 2015 OSA

16. X. Xu, W. Huang, and M. Xu, "Orthogonal polynomials describing polarization aberration for lithographic lens with CaF_2 material," (submitted) (2015).
17. M. Laikin, *Lens Design* (CRC, 2007), Chap. 11.

1. Introduction

Optical lithography has approached a regime of high numerical aperture (NA) and wide field, and polarized illumination has become a viable technique to improve imaging quality. However, factors such as lens material inhomogeneity, surfaces scattering, intrinsic and stress-induced birefringence, and lens coatings can potentially alter the polarization state of light to some degree [1]. The transmission difference (i.e., diattenuation) and phase shift (i.e., retardance) between the s- and p-polarization components of rays that pass through an optical interface are called polarization aberration (PA) [2], which can cause process window degradation, critical dimension variation, and pattern placement error.

PA can be represented by a Jones matrix, and all of the Jones matrices on the exit pupil form a Jones pupil. Although a Jones pupil provides a full and accurate description for PA, it lacks visualization. Some researchers have attempted to improve the intuition of Jones matrices. Chipman [3] and McGuire [4] derived the PA distribution on the exit pupil in terms of the incidence angles of chief and marginal ray through paraxial approximation. Totzeck [5] presented a decomposition of the Jones pupil by using "Jones Zernikes". McIntyre [6] represented the Jones matrix by Pauli matrices and conducted a comprehensive comparison of Pauli representation versus Jones representation. Geh [7] utilized single value decomposition (SVD) to break down a Jones matrix into five parts, namely, wavefront, apodization, diattenuation, retardance, and rotation. Ruoff and Totzeck [8,9] proposed orientation Zernike polynomials (OZP) to decompose the diattenuation and retardance further. However, most of these studies focused on the distribution rule of PA on the pupil, and little attention has been paid to the field. The PA of a lithographic lens with high NA can be measured [10,11] and compensated [12,13] nowadays, and the two main characteristics of modern lithographic lenses are high NA and wide field. Thus, the measurement and compensation of PA must be operated over a wide field. So, revealing the distribution rule of PA on the field is significant. Without using Jones pupil, Sasian [14] provided a proper way to understand PAs by the concepts of polarization fields and of wavefronts of two sheets. In this paper, we propose an alternative method based on the OZP to reveal the distribution rules of PA on both the pupil and the field.

2. Establishment of Field-orientation Zernike polynomials

The coordinate system is shown in Fig. 1. The polar coordinates of the field on the object plane and the exit pupil are (h, α) and (ρ, θ), respectively.

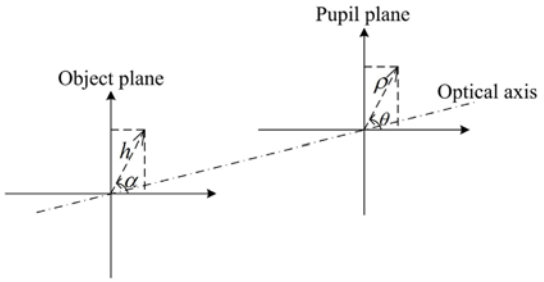

Fig. 1. Coordinate system.

By SVD, the Jones matrix J can be defined in terms of physical properties, i.e., a homogeneous partial polarizer J_{pol}, a homogeneous pure retarder J_{ret}, mean transmittance t, and mean scalar phase Φ, as shown in Eq. (1):

$$J = te^{i\Phi} J_{pol}(d, \psi_p, \delta_p) \cdot J_{ret}(\phi, \psi_r, \delta_r), \tag{1}$$

#248659 Received 27 Aug 2015; revised 25 Sep 2015; accepted 30 Sep 2015; published 14 Oct 2015
© 2015 OSA

where J_{pol} represents the diattenuation, J_{ret} represents the retardance; d, ϕ, ψ_p, and ψ_r represent the diattenuation value, retardance value, bright axis direction and fast axis direction, respectively; and δ_p and δ_r represent the ellipticity of the diattenuaton and retardance, respectively. δ_p and δ_r are reportedly very small and can be safely neglected for modern lithographic lenses [7]. J_{pol} and J_{ret} can be expressed as [8]:

$$J_{pol}(d,\psi_p)=\begin{pmatrix}1+d\cos 2\psi_p & d\sin 2\psi_p\\ d\sin 2\psi_p & 1-d\cos 2\psi_p\end{pmatrix}, \tag{2}$$

$$J_{ret}(\phi,\psi_r)=\begin{pmatrix}\cos\phi-i\sin\phi\cos 2\psi_r & -i\sin\phi\sin 2\psi_r\\ -i\sin\phi\sin 2\psi_r & \cos\phi+i\sin\phi\cos 2\psi_r\end{pmatrix}. \tag{3}$$

We use OZP to decompose the diattenuation and retardance further:

$$J_{pol}=I+\sum_{j=1}^{\infty}C_j\cdot OZ_j,\quad J_{ret}=\cos\phi I-i\sum_{j=1}^{\infty}C_j\cdot OZ_j, \tag{4}$$

where I is the 2 × 2 unit matrix, C_j is the OZP coefficient, and OZ_j is the OZP term, which is defined as

$$OZ_j=OZ_{n,\varepsilon}^{m}=R_n^m(\rho)O_\varepsilon^m(\theta), \tag{5}$$

where ε = 0 or 1, and $R_n^m(\rho)$ indicates the radial part, which is the same as the radial part of Zernike polynomials. The angular part $O_\varepsilon^m(\theta)$ is defined as

$$O_0^m(\theta)=\begin{pmatrix}\cos m\theta & \sin m\theta\\ \sin m\theta & -\cos m\theta\end{pmatrix}, O_1^m(\theta)=\begin{pmatrix}\sin m\theta & -\cos m\theta\\ -\cos m\theta & -\sin m\theta\end{pmatrix}. \tag{6}$$

Instead of using the three indices n, m, and ε to label a certain OZP term, a numbering scheme is clearly discussed to label $OZ_{n,\varepsilon}^{m}$ as OZ_j in a previous study [8]. The first 20 terms of OZP are listed in Table 3 in Appendix A. OZP terms arranged according to their symmetry properties are shown in Fig. 2, where the color and the short line represent the positive eigenvalue and the corresponding direction of the eigen polarization state, respectively.

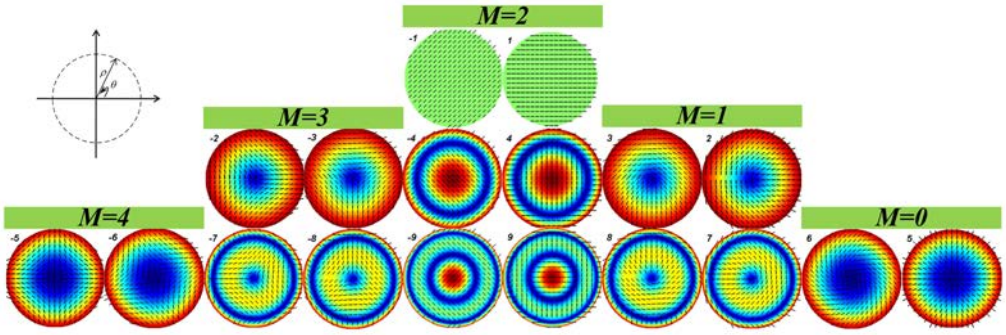

Fig. 2. OZP arranged according to symmetry properties.

PAs of different fields have different OZP coefficients, thus C_j is a function of field coordinates, $C_j = C_j(h,\alpha)$, which can be expanded by Fringe Zernike polynomials (FZP):

$$C_j(h,\alpha)=\sum_{i=1}^{\infty}a_i\cdot F_i(h,\alpha), \tag{7}$$

#248659 Received 27 Aug 2015; revised 25 Sep 2015; accepted 30 Sep 2015; published 14 Oct 2015
© 2015 OSA

where a_i is the coefficient, and F_i is the FZP term, as shown in Table 4 in Appendix B, that can be written as $F_{n',\varepsilon'}^{m'}$ to clearly show the angular parameter m' and radial parameter n':

$$F_{n',0}^{m'}(h,\alpha)=R_{n'}^{m'}(h)\cos m'\alpha,\ \ F_{n',1}^{m'}(h,\alpha)=R_{n'}^{m'}(h)\sin m'\alpha. \tag{8}$$

Thus, $C_j \cdot OZ_j$ can be expanded as

$$C_j\cdot OZ_j=(\sum_{n'=0}^{\infty}\sum_{m'=0}^{n}\sum_{\varepsilon'=0}^{1}a_{m'n'\varepsilon'}\cdot F_{n',\varepsilon'}^{m'})\cdot(\sum_{n=0}^{\infty}\sum_{m=-n}^{n}\sum_{\varepsilon=0}^{1}OZ_{n,\varepsilon}^{m}). \tag{9}$$

In the polynomials in Eq. (9), four basic formulas are present, namely, $F_{n',0}^{m'}\cdot OZ_{n,0}^{m}$, $F_{n',1}^{m'}\cdot OZ_{n,0}^{m}$, $F_{n',0}^{m'}\cdot OZ_{n,1}^{m}$, and $F_{n',1}^{m'}\cdot OZ_{n,1}^{m}$. They can be equivalently transformed into another four basic formulas f_{0+}, f_{0-}, f_{1+}, and f_{1-}:

$$\begin{aligned} f_{0+}&=F_{n',0}^{m'}OZ_{n,0}^{m}+F_{n',1}^{m'}OZ_{n,1}^{m},\quad f_{0-}=F_{n',0}^{m'}OZ_{n,0}^{m}-F_{n',1}^{m'}OZ_{n,1}^{m},\\ f_{1+}&=F_{n',1}^{m'}OZ_{n,0}^{m}+F_{n',0}^{m'}OZ_{n,1}^{m},\quad f_{1-}=-F_{n',1}^{m'}OZ_{n,0}^{m}+F_{n',0}^{m'}OZ_{n,1}^{m}. \end{aligned} \tag{10}$$

For rotationally symmetric systems, the PA distribution on the pupil and the field is rotationally symmetric along the optical axis. Therefore, the polynomials used to describe PA should also be rotationally symmetric. Formula (10) is rotationally symmetric, indicating that the distributions of both its eigenvalues and eigenvector directions are rotationally symmetric. The eigenvalue and eigenvector of the diattenuation (retardance) represent the diattenuation (retardance) value and the direction of the bright (fast) axis, respectively.

The eigenvalue of f_{0+} is $R_{n'}^{m'}(h)R_n^m(\rho)$, which is a function of the radial coordinates h and ρ, and independent of the angular coordinates θ and α. When the angular coordinates changes, the eigenvalue stays unchanged. Thus, the eigenvalue is rotationally symmetric. The corresponding eigenvector is

$$\mathrm{E}_{0+}=\begin{pmatrix}\cos\dfrac{m\theta-m'\alpha}{2}\\ \sin\dfrac{m\theta-m'\alpha}{2}\end{pmatrix}. \tag{11}$$

We rotate E_{0+} by an arbitrary angle β and require it to be the same with the original one obtained at the shifted angular coordinate position ($\theta+\beta$, $\alpha+\beta$), i.e.,

$$\frac{m\theta-m'\alpha}{2}+\beta=\frac{m}{2}(\theta+\beta)-\frac{m'}{2}(\alpha+\beta). \tag{12}$$

Then, we obtain $m - m' = 2$. Under this condition, f_{0+} is rotationally symmetric. Similarly, we obtain $m + m' = 2$, $m + m' = 2$, and $m - m' = 2$ for f_{0-}, f_{1+}, and f_{1-}, respectively. Note that m is an integer and m' is a non-negative integer.

Then, a set of rotationally symmetric polynomials is obtained. Each term of the polynomials is a 2 × 2 matrix, and is a function of the pupil and field coordinates. The polynomials can be used to describe the PA distribution on the pupil and the field simultaneously. We name the polynomials "Field-orientation Zernike polynomials (FOZP)". The first 26 terms of FOZP are shown in Table 1, where different terms of FOZP are labeled as FOZ_j. The product of FOZ_j and FOZ_i follows Eq. (13):

$$\pi^{-2}4^{\frac{-1}{1+\delta_{m'0}}}\int_0^{2\pi}\int_0^1\int_0^{2\pi}\int_0^1(FOZ_i\cdot FOZ_j+FOZ_j\cdot FOZ_i)\rho\cdot d\rho\cdot d\theta\cdot h\cdot dh\cdot d\alpha=\begin{cases}I & \text{when } i=j;\\ \boldsymbol{0} & \text{others.}\end{cases} \tag{13}$$

where $\boldsymbol{0}$ denotes the 2 × 2 zero matrix, $\delta_{m'0}$ is the Kronecker delta function. Equation (19) is defined as the orthogonality property of FOZP. Different terms of FOZP are orthogonal. Figure 3 shows the field maps of FOZP.

#248659 Received 27 Aug 2015; revised 25 Sep 2015; accepted 30 Sep 2015; published 14 Oct 2015
© 2015 OSA

Table 1. First 26 terms of Field-orientation Zernike polynomials

j	m	n	m'	n'	f	FOZ_j	j	m	n	m'	n'	f	FOZ_j
1	0	0	2	2	0–	$F_5{\cdot}OZ_1 + F_6{\cdot}OZ_{-1}$	14	1	3	1	1	1 +	$F_3{\cdot}OZ_7 + F_2{\cdot}OZ_8$
2	0	0	2	2	1 +	$F_6{\cdot}OZ_1 - F_5{\cdot}OZ_{-1}$	15	1	3	1	3	0–	$F_7{\cdot}OZ_7 - F_8{\cdot}OZ_8$
3	1	1	1	1	0–	$F_2{\cdot}OZ_2 - F_3{\cdot}OZ_3$	16	1	3	1	3	1 +	$F_8{\cdot}OZ_7 + F_7{\cdot}OZ_8$
4	1	1	1	1	1 +	$F_3{\cdot}OZ_2 + F_2{\cdot}OZ_3$	17	0	4	2	2	0–	$F_5{\cdot}OZ_9 + F_6{\cdot}OZ_{-9}$
5	0	2	2	2	0–	$F_5{\cdot}OZ_4 + F_6{\cdot}OZ_{-4}$	18	0	4	2	2	1 +	$F_6{\cdot}OZ_9 - F_5{\cdot}OZ_{-9}$
6	0	2	2	2	1 +	$F_6{\cdot}OZ_4 - F_5{\cdot}OZ_{-4}$	19	0	0	2	4	0–	$F_{12}{\cdot}OZ_1 + F_{13}{\cdot}OZ_{-1}$
7	2	2	0	0	0–	OZ_5	20	0	0	2	4	1 +	$F_{13}{\cdot}OZ_1 - F_{12}{\cdot}OZ_{-1}$
8	2	2	0	0	1 +	OZ_6	21	3	3	1	1	0 +	$F_2{\cdot}OZ_{10} + F_3{\cdot}OZ_{11}$
9	2	2	0	2	0–	$F_4{\cdot}OZ_5$	22	3	3	1	1	1–	$-F_3{\cdot}OZ_{10} + F_2{\cdot}OZ_{11}$
10	2	2	0	2	1 +	$F_4{\cdot}OZ_6$	23	–1	1	3	3	0–	$F_{10}{\cdot}OZ_{-2} + F_{11}{\cdot}OZ_{-3}$
11	1	1	1	3	0–	$F_7{\cdot}OZ_2 - F_8{\cdot}OZ_3$	24	–1	1	3	3	1 +	$F_{11}{\cdot}OZ_{-2} - F_{10}{\cdot}OZ_{-3}$
12	1	1	1	3	1 +	$F_8{\cdot}OZ_2 + F_7{\cdot}OZ_3$	25	3	3	1	3	0 +	$F_7{\cdot}OZ_{10} + F_8{\cdot}OZ_{11}$
13	1	3	1	1	0–	$F_2{\cdot}OZ_7 - F_3{\cdot}OZ_8$	26	3	3	1	3	1–	$-F_8{\cdot}OZ_{10} + F_7{\cdot}OZ_{11}$

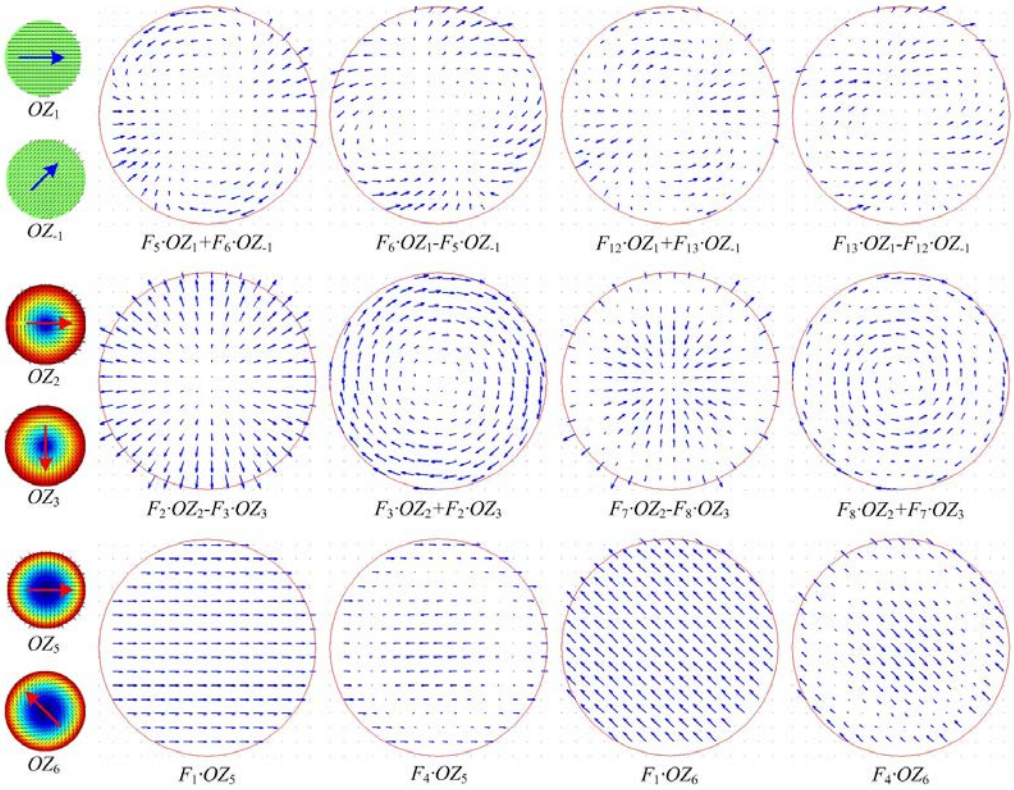

Fig. 3. Samples of field maps of FOZP.

The names of FOZP terms are listed in Table 2. The nomenclature for PA used in this paper was first proposed by Chipman [3] and then improved by McGuire [4]. According to this nomenclature, PAs are viewed as vector terms and named after the wavefront aberrations with the same field height and pupil radius dependencies. To some extent, the nomenclature provides physical insights into what the FOZP terms represent.

#248659 Received 27 Aug 2015; revised 25 Sep 2015; accepted 30 Sep 2015; published 14 Oct 2015
© 2015 OSA

Table 2. Names of FOZP terms

FOZP	Name
$F_5{\cdot}OZ_1 + F_6{\cdot}OZ_{-1}$; $F_6{\cdot}OZ_1 - F_5{\cdot}OZ_{-1}$	Vector Piston (2nd order)
$F_2{\cdot}OZ_2 - F_3{\cdot}OZ_3$; $F_3{\cdot}OZ_2 + F_2{\cdot}OZ_3$	Vector Tilt
$F_5{\cdot}OZ_4 + F_6{\cdot}OZ_{-4}$; $F_6{\cdot}OZ_4 - F_5{\cdot}OZ_{-4}$	Vector Astigmatism (4th order)
OZ_5; OZ_6	Vector Defocus
$F_4{\cdot}OZ_5$; $F_4{\cdot}OZ_6$	Vector Field Curvature
$F_7{\cdot}OZ_2 - F_8{\cdot}OZ_3$; $F_8{\cdot}OZ_2 + F_7{\cdot}OZ_3$	Vector Distortion
$F_2{\cdot}OZ_7 - F_3{\cdot}OZ_8$; $F_3{\cdot}OZ_7 + F_2{\cdot}OZ_8$	Vector Coma (4th order)
$F_7{\cdot}OZ_7 - F_8{\cdot}OZ_8$; $F_8{\cdot}OZ_7 + F_7{\cdot}OZ_8$	Vector Coma (6th order)
$F_5{\cdot}OZ_9 + F_6{\cdot}OZ_{-9}$; $F_6{\cdot}OZ_9 - F_5{\cdot}OZ_{-9}$	Vector Astigmatism (6th order)
$F_{12}{\cdot}OZ_1 + F_{13}{\cdot}OZ_{-1}$; $F_{13}{\cdot}OZ_1 - F_{12}{\cdot}OZ_{-1}$	Vector Piston (4th order)
$F_2{\cdot}OZ_{10} + F_3{\cdot}OZ_{11}$; $-F_3{\cdot}OZ_{10} + F_2{\cdot}OZ_{11}$	Vector Coma (4th order)
$F_{10}{\cdot}OZ_{-2} + F_{11}{\cdot}OZ_{-3}$; $F_{11}{\cdot}OZ_{-2} - F_{10}{\cdot}OZ_{-3}$	Vector 3 foil (4th order)
$F_7{\cdot}OZ_{10} + F_8{\cdot}OZ_{11}$; $-F_8{\cdot}OZ_{10} + F_7{\cdot}OZ_{11}$	Vector Coma (6th order)

3. Simulation

In this section, two lenses are used for simulation to verify FOZP. The purpose of simulation is to assess what the distribution rule of PA on the field really is. Figure 4 shows the simulation flowchart. First, the polarization ray tracing function in the software Code V is used to obtain the Jones pupils for all the field points. Second, the Jones pupil is decomposed by SVD, and the diattenuation and retardance are obtained. Third, the diattenuation and retardance are fitted by OZP. Finally, the coefficient of each OZP term, i.e., $C_j(h,\alpha)$, is further fitted by FZP.

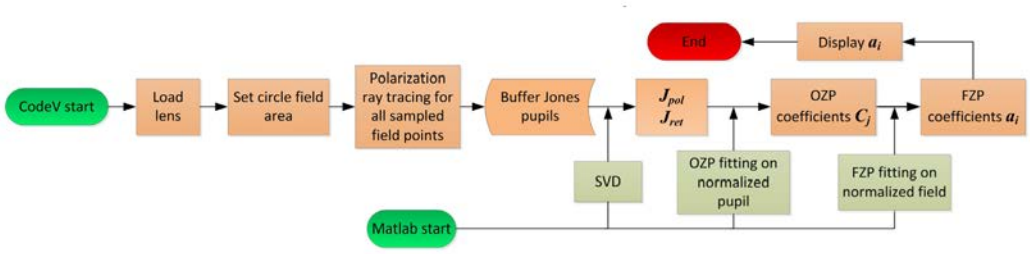

Fig. 4. Simulation flowchart.

3.1 High-NA lithographic lens

A water-immersion ArF lithographic lens of NA 1.35 [15] with anti-reflective (AR) and high-reflective (HR) coatings is used for simulation. The lens material is SiO_2, and the lens is rotationally symmetric. Figure 5 shows the lens drawing and the optical properties of the AR and the HR coatings. Figure 6 shows the simulation results.

Results show that different OZP terms and their coefficients can always be combined as rotationally symmetric FOZP terms. For example, the F_5 coefficient of C_1 is equal to the F_6 coefficient of C_{-1}. Thus, they can be combined as $F_5{\cdot}OZ_1 + F_6{\cdot}OZ_{-1}$ and share the same coefficient. Other combinations produce $F_2{\cdot}OZ_2 - F_3{\cdot}OZ_3$, $F_5{\cdot}OZ_1 + F_6{\cdot}OZ_{-1}$, $F_5{\cdot}OZ_4 + F_6{\cdot}OZ_{-4}$, $F_1{\cdot}OZ_5$, etc. The FOZP terms are marked in the red rectangles on Fig. 6, which are in accordance with Table 1. The simulation results agree with FOZP theory.

It should be noted that the field area used for simulation is a circle of radius 64 mm on the object plane, whereas the work field area of the lithographic lens is a rectangle with an area of 104 mm × 22 mm. The work field can be viewed as a rectangular part of the circle. Thus, the distribution rule of PA on the circle field applies to that on the work field area.

When the material CaF_2 is used in the lithographic lens, the retardance is no longer rotationally symmetric because of the intrinsic birefringence of CaF_2. Another set of

#248659 Received 27 Aug 2015; revised 25 Sep 2015; accepted 30 Sep 2015; published 14 Oct 2015
© 2015 OSA

orthogonal polynomials is established for this circumstance, as presented in a subsequent paper [16].

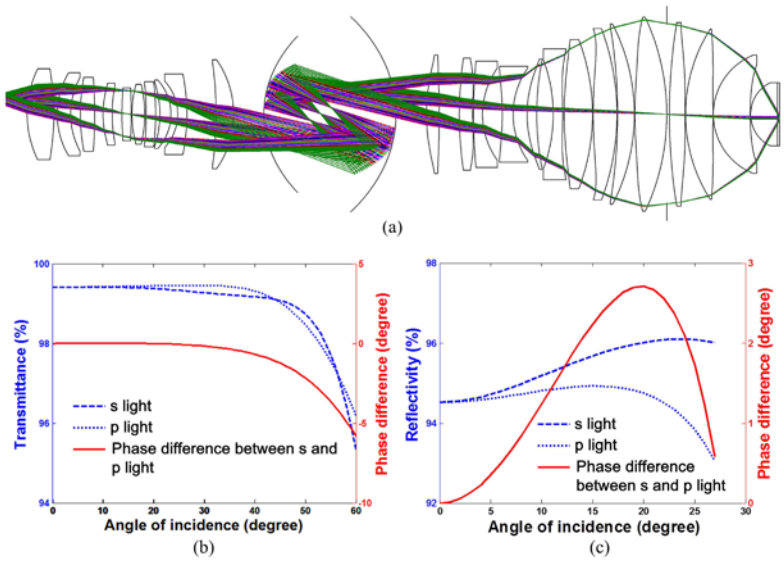

Fig. 5. (a) A NA 1.3 lithographic lens; (b) Transmittance and phase difference of s and p light of AR coating; (d) Reflectivity and phase difference of s and p light of HR coating.

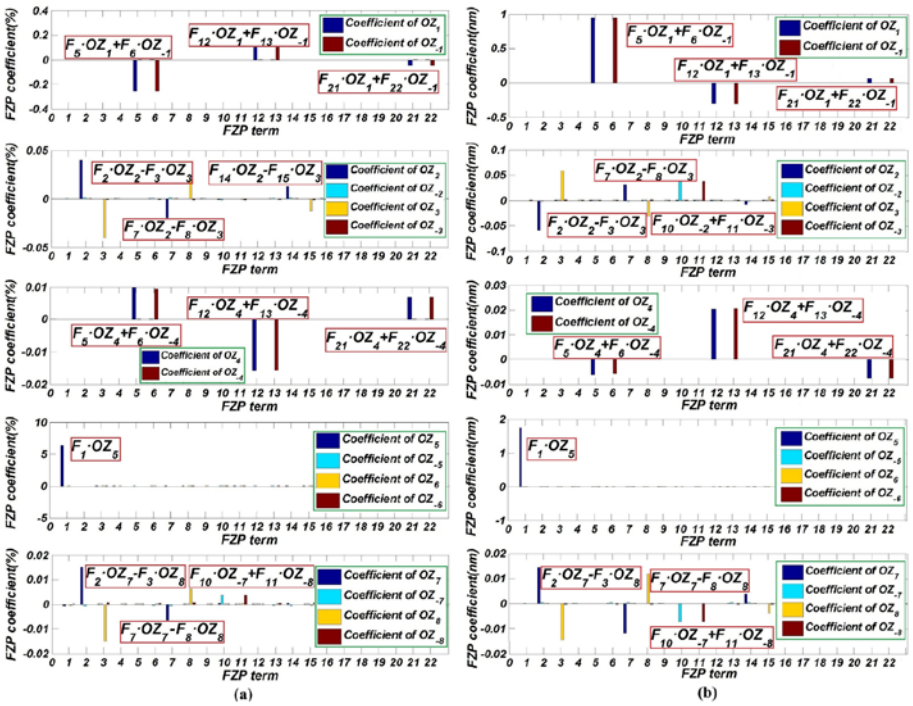

Fig. 6. Simulation results of lithographic lens. (a) Diattenuation; (b) Retardance.

#248659 Received 27 Aug 2015; revised 25 Sep 2015; accepted 30 Sep 2015; published 14 Oct 2015
© 2015 OSA

3.2 High-NA microscope objective

Except for lithographic lens, FOZP can be used for other rotationally symmetric optical systems. In this part, an oil-immersion microscope objective of NA 1.28 [17] with AR coatings is used for simulation. The objective drawing and the optical property of the AR coating are shown in Fig. 7. The simulation results are shown in Fig. 8.

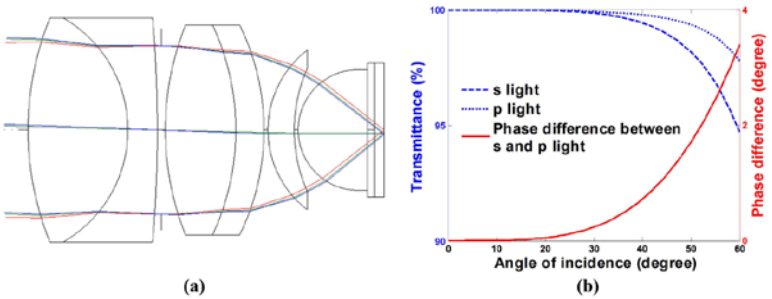

Fig. 7. (a) A NA 1.28 microscope objective; (b) Transmittance and phase difference of s and p light of AR coating.

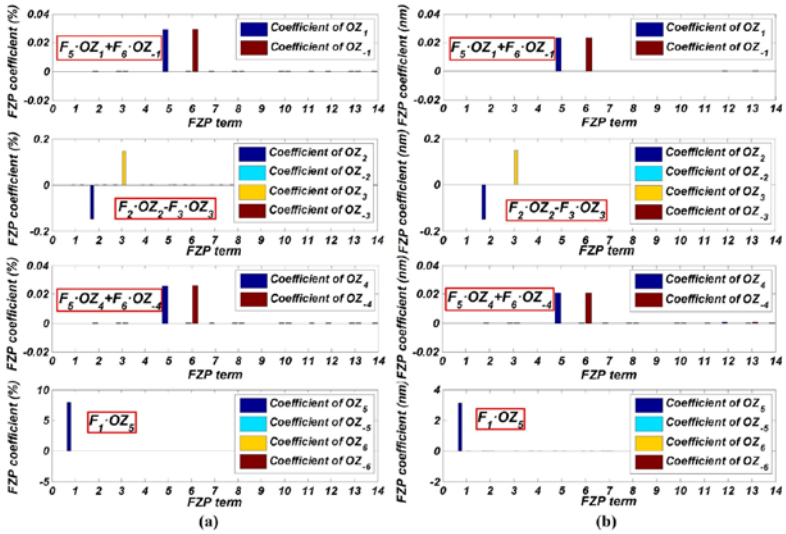

Fig. 8. Simulation results of microscope objective. (a) Diattenuation; (b) Retardance.

Results show that different OZP terms and their coefficients can also be combined as rotationally symmetric FOZP terms. While, the FOZP order of microscope objective is smaller than lithographic lens, because the field area of microscope objective is a circle of radius 8 mm on the object plane, which is smaller than that of lithographic lens.

5. Conclusion

We propose a new set of polynomials, FOZP, to describe the PA of rotationally symmetric optical systems. The polynomials are orthonormal to each other, and can simultaneously reveal the distribution rules of PA on the pupil and the field. FOZP have many potential applications in the measurement and compensation of PA. A NA 1.35 lithographic lens and a NA 1.28 microscope objective are used to verify FOZP. The simulation results show what the distribution rule of polarization aberration actually is on the field, which coincide with the distribution rule provided by FOZP. Further research will extend FOZP from rotationally symmetric to n-fold to describe the retardance of lithographic lens with CaF_2 material.

#248659 Received 27 Aug 2015; revised 25 Sep 2015; accepted 30 Sep 2015; published 14 Oct 2015
© 2015 OSA

Appendix A

Table 3. The first 20 terms of orientation Zernike polynomials

j	OZ_j	j	OZ_j
1	$\begin{pmatrix}1 & 0\\ 0 & -1\end{pmatrix}$	6	$\sqrt{6}\rho^2\begin{pmatrix}\sin 2\theta & -\cos 2\theta\\ -\cos 2\theta & -\sin 2\theta\end{pmatrix}$
–1	$\begin{pmatrix}0 & 1\\ 1 & 0\end{pmatrix}$	–6	$\sqrt{6}\rho^2\begin{pmatrix}\sin 2\theta & \cos 2\theta\\ \cos 2\theta & -\sin 2\theta\end{pmatrix}$
2	$2\rho\begin{pmatrix}\cos\theta & \sin\theta\\ \sin\theta & -\cos\theta\end{pmatrix}$	7	$\sqrt{8}(3\rho^3-2\rho)\begin{pmatrix}\cos\theta & \sin\theta\\ \sin\theta & -\cos\theta\end{pmatrix}$
–2	$2\rho\begin{pmatrix}\cos\theta & -\sin\theta\\ -\sin\theta & -\cos\theta\end{pmatrix}$	–7	$\sqrt{8}(3\rho^3-2\rho)\begin{pmatrix}\cos\theta & -\sin\theta\\ -\sin\theta & -\cos\theta\end{pmatrix}$
3	$2\rho\begin{pmatrix}\sin\theta & -\cos\theta\\ -\cos\theta & -\sin\theta\end{pmatrix}$	8	$\sqrt{8}(3\rho^3-2\rho)\begin{pmatrix}\sin\theta & -\cos\theta\\ -\cos\theta & -\sin\theta\end{pmatrix}$
–3	$2\rho\begin{pmatrix}\sin\theta & \cos\theta\\ \cos\theta & -\sin\theta\end{pmatrix}$	–8	$\sqrt{8}(3\rho^3-2\rho)\begin{pmatrix}\sin\theta & \cos\theta\\ \cos\theta & -\sin\theta\end{pmatrix}$
4	$\sqrt{3}(2\rho^2-1)\begin{pmatrix}1 & 0\\ 0 & -1\end{pmatrix}$	9	$\sqrt{5}(6\rho^4-6\rho^2+1)\begin{pmatrix}1 & 0\\ 0 & -1\end{pmatrix}$
–4	$\sqrt{3}(2\rho^2-1)\begin{pmatrix}0 & 1\\ 1 & 0\end{pmatrix}$	–9	$\sqrt{5}(6\rho^4-6\rho^2+1)\begin{pmatrix}0 & 1\\ 1 & 0\end{pmatrix}$
5	$\sqrt{6}\rho^2\begin{pmatrix}\cos 2\theta & \sin 2\theta\\ \sin 2\theta & -\cos 2\theta\end{pmatrix}$	10	$\sqrt{8}\rho^3\begin{pmatrix}\cos 3\theta & \sin 3\theta\\ \sin 3\theta & -\cos 3\theta\end{pmatrix}$
–5	$\sqrt{6}\rho^2\begin{pmatrix}\cos 2\theta & -\sin 2\theta\\ -\sin 2\theta & -\cos 2\theta\end{pmatrix}$	–10	$\sqrt{8}\rho^3\begin{pmatrix}\cos 3\theta & -\sin 3\theta\\ -\sin 3\theta & -\cos 3\theta\end{pmatrix}$

Appendix B

Table 4. Fringe Zernike polynomials of field coordinates

j	F_j	j	F_j
1	1	17	$\sqrt{10}h^4\cos 4\alpha$
2	$2h\cos\alpha$	18	$\sqrt{10}h^4\sin 4\alpha$
3	$2h\sin\alpha$	19	$\sqrt{12}(5h^5-4h^3)\cos 3\alpha$
4	$\sqrt{3}(2h^2-1)$	20	$\sqrt{12}(5h^5-4h^3)\sin 3\alpha$
5	$\sqrt{6}h^2\cos 2\alpha$	21	$\sqrt{14}(15h^6-20h^4+6h^2)\cos 2\alpha$
6	$\sqrt{6}h^2\sin 2\alpha$	22	$\sqrt{14}(15h^6-20h^4+6h^2)\sin 2\alpha$
7	$\sqrt{8}(3h^3-2h)\cos\alpha$	23	$\sqrt{16}(35h^7-60h^5+30h^3-4h)\cos\alpha$
8	$\sqrt{8}(3h^3-2h)\sin\alpha$	24	$\sqrt{16}(35h^7-60h^5+30h^3-4h)\sin\alpha$
9	$\sqrt{5}(6h^4-6h^2+1)$	25	$\sqrt{9}(70h^8-140h^6+90h^4-20h^2+1)$
10	$\sqrt{8}h^3\cos 3\alpha$	26	$\sqrt{10}h^5\cos 5\alpha$
11	$\sqrt{8}h^3\sin 3\alpha$	27	$\sqrt{10}h^5\sin 5\alpha$
12	$\sqrt{10}(4h^4-3h^2)\cos\alpha$	28	$\sqrt{14}(6h^6-5h^4)\cos 4\alpha$
13	$\sqrt{10}(4h^4-3h^2)\sin\alpha$	29	$\sqrt{14}(6h^6-5h^4)\sin 4\alpha$
14	$\sqrt{12}(10h^5-12h^3+3h)\cos\alpha$	30	$\sqrt{16}(21h^7-30h^5+10h^3)\cos 3\alpha$
15	$\sqrt{12}(10h^5-12h^3+3h)\sin\alpha$	31	$\sqrt{16}(21h^7-30h^5+10h^3)\sin 3\alpha$
16	$\sqrt{7}(20h^6-30h^4+12h^2-1)$		

#248659 Received 27 Aug 2015; revised 25 Sep 2015; accepted 30 Sep 2015; published 14 Oct 2015
© 2015 OSA